

Article

# Zeta Potential of Pyrite Particles in Concentrated Solutions of Monovalent Seawater Electrolytes and Amyl Xanthate

Alvaro Paredes <sup>1</sup>, Sergio M. Acuña <sup>2,\*</sup> , Leopoldo Gutiérrez <sup>3</sup> and Pedro G. Toledo <sup>1,\*</sup>

<sup>1</sup> Department of Chemical Engineering and Laboratory of Surface Analysis (ASIF), University of Concepción, P.O. Box 160-C, Correo 3, 4030000 Concepción, Chile; aparedesg@udec.cl

<sup>2</sup> Department of Food Engineering, Universidad del Bio-Bio, P.O. Box 447, 3780000 Chillán, Chile

<sup>3</sup> Department of Metallurgical Engineering, Universidad de Concepción, PO Box 160-C, Correo 3, 4030000 Concepción, Chile; lgutierrezb@udec.cl

\* Correspondence: sacuna@ubiobio.cl (S.M.A.); petoledo@udec.cl (P.G.T.);  
Tel.: +56-42-2463172 (S.M.A.); +56-41-2203658 (P.G.T.)

Received: 10 July 2019; Accepted: 7 August 2019; Published: 27 September 2019



**Abstract:** Charge screening and adsorption capacity of monovalent ions onto pyrite (Py) in aqueous suspensions and the effect of potassium amyl xanthate (PAX) has been studied by measuring the changes in zeta potential (z<sub>p</sub>) versus pH with streaming potential. PAX addition in the absence of salts leads to an increase in |z<sub>p</sub>| suggesting dissolution of the surface ferric hydroxides and recovery of bare Py, corroborating existing theories. In the presence of salt, addition of PAX at pH > 6, for which hydroxides interference is not expected, has little effect over the z<sub>p</sub>, except when Li is present. The water network around the polar head of PAX is expected to be similar to that of hydrated Li<sup>+</sup> facilitating the linkage between them and, thus, the formation of Li-mediated Py–PAX bridges. We speculate that these bridges lead to a xanthate shield around anionic sites on Py, decreasing |z<sub>p</sub>|. An increased PAX dose amplifies the effect of Li as a Py activator but only at low salt. At high salt concentrations, >0.01 M, PAX molecules do not find room to percolate to the surface of Py. Results for monovalent cations should improve our understanding of copper flotation processes in the presence of Py in saltwater.

**Keywords:** pyrite; seawater; PAX; adsorption; zeta potential; viscosity

## 1. Introduction

The use of seawater in mining processes is becoming mandatory in regions where freshwater is scarce. The need for water is so great that the use of seawater is decided long before having a fair comprehension of the effects of the various electrolytes and the buffer condition of seawater in the processes involved, particularly in pyrite flotation [1]. Pyrite oxidation and collector adsorption have long been studied and the literature is full of important contributions [2–15]. Pyrite under argon atmosphere, which according to Fornasiero et al. [7] is the closest to a native state, has a negative surface potential over a wide range of pH, with an isoelectric point at ca. pH 1.2 ± 0.4, a value slightly lower than the value measured by Healy et al. [3], ca. pH 2. This negative potential is thought to be a consequence of a sulfur-rich surface with an iron-deficient sulfide lattice. Pyrite exposed to deuterated water (D<sub>2</sub>O) alone shows no evidence of oxidation products on its surface, however in air or aqueous solution, pyrite becomes rapidly oxidized forming hydrophilic oxide/hydroxides and hydrophobic iron-deficient sulfide surfaces [16–19]. The hydrophilic species prevent significant flotation without the addition of collector, which is verified by the easy flotation that is obtained when complexing surface iron with EDTA in solution [10,19]. In a mildly acidic solution, a soluble iron product is

formed, leaving a surface sulfur species, very likely elemental sulfur [4,8]. In alkaline solution, ferric hydroxide, sulfate species, and iron-deficient sulfide are formed. Undoubtedly, the most used collector for the flotation of sulfide minerals belongs to the series of xanthates. The earliest theories of xanthate adsorption on pyrite surfaces involved the formation of any of the following four species: Adsorbed xanthate, metal xanthate, elemental sulfur and/or polysulfide, and dixanthogen, each contributing to the hydrophobicity of the surface (for reviews, see Smart et al. [10,19]). A refined and more recent theory by López Valdivieso et al. [12] involved adsorption of xanthate at specific non-oxidized surface sites of pyrite, anodic oxidation of xanthate adsorbed ions to dixanthogen, and a cathodic reaction at oxidized surface sites where ferric hydroxide is reduced to  $\text{Fe}^{2+}$  ions. According to the same authors, the resulting  $\text{Fe}^{2+}$  ions can be hydrolyzed and/or oxidized to  $\text{Fe}^{3+}$  species depending on conditions. In parallel, Mermillod-Blondin et al. [11] presented an alternative theory in which xanthate is adsorbed as a mixture of iron-xanthate complex and dixanthogen at pillar structures of oxidized species, such as iron hydroxides and iron oxyhydroxides, on the pyrite surface. In highly oxidized pyrite, it is likely that both theories apply. The effect of ions such as  $\text{Cu}^{2+}$ ,  $\text{Fe}^{2+}$ , and  $\text{Ca}^{2+}$  on the floatability of pyrite has been studied extensively [20–23]; in particular, the activation that these ions impart in pyrite increases the adsorption of xanthate and ultimately the recovery of pyrite within the pH range 6–10. The effect of the number of seawater ions, however, presents a new scenario that probably requires reviewing existing theories about the mechanisms of pyrite oxidation, collector adsorption, and reaction mechanisms. As a first step, we study the effect of electrolytes from the monovalent series Li, Na, K, and Cs on the zeta potential of pyrite and the effect of electrolyte concentration. We also study the effect on the zeta potential of pyrite conditioned in saltwater when xanthate (potassium amyl xanthate) is added.

## 2. Materials and Methods

High-grade pyrite (Ward's Science) from a Peruvian mine was used. X-ray diffraction analysis showed that pyrite was the only mineralogical phase present in the sample. Fluorescence spectroscopy analysis indicated a 54.2% S and 44.3% Fe (wt.%) with 1.5% impurities (0.06% Mg, 0.24%  $\text{Al}_2\text{O}_3$ , 0.24%  $\text{SiO}_2$ , 0.07% P, 0.4% Ca, 0.21% Cu, 0.08% Zn, 0.15% As). Pyrite samples were prepared under mild oxidation conditions and preserved in nitrogen at low temperature for further use. Pyrite was ground under a nitrogen atmosphere in a planetary mill with tungsten carbide balls to prevent the typical oxidation that occurs in the grinding process due to the use of steel balls; the powder obtained was then sieved to a size of  $<44\ \mu\text{m}$  (mesh 325) and ran through a magnetic separation. Solution preparation and zeta potential measurements were all performed in a nitrogen glove box. Water was deoxygenated by cycles of boiling at atmospheric pressure. Pyrite suspensions were prepared at 1% solids (wt.%) in ultra-pure deoxygenated water Milli-Q (18.2 M $\Omega\text{cm}$ ) for zeta potential measurements. Analytical grade LiCl, NaCl, KCl, and CsCl (Merck) was added to the pyrite suspensions at concentrations of 0.01, 0.05, and 0.1 M. Potassium amyl xanthate or PAX (ORICA) was used in concentration of  $10^{-4}$  and  $10^{-3}$  M. PAX was further purified by dissolution in acetone and precipitation by ether. Conditioning of the pyrite sample involves 5 min with the electrolytes at the pH of the experiment, and additional 10 min with PAX at the same pH. Zeta potential of pyrite was evaluated by streaming potential method (Stabino, Microtrac) in titration mode, adjusting the pH along the measurements. The key part of the Stabino is a cylindrical PTFE chamber with an oscillating piston, both carrying only very little anionic charge at the surface. A fraction of the particles in the cell was immobilized at the surface of the wall. Therefore, with the piston movement, the mobile cloud of the double layer of the immobilized particles was pushed up and down. That oscillating ion cloud produced an alternating voltage at the two electrodes, the streaming potential, which is proportional to the zeta potential of the particles. This zeta potential technique implemented in the Stabino has been used recently and successfully in various applications of interest in mineral processing [24–27]. The solution pH was adjusted with analytical grade KOH, NaOH, LiOH, and CsOH, at a concentration of 0.5 M (Merck) and HCl 0.020 M (Merck), the latter in order to not introduce a base other than  $\text{Cl}^-$ ; this disparity in concentration is to achieve an alkaline pH without using too much base and to have a slow and controlled evolution of the zeta

potential to the acid pH. The zeta potential versus pH curves presented in this work correspond to an average of at least three to five curves; error bars corresponding to deviations from the average value were also calculated and reported.

### 3. Results and Discussion

#### 3.1. Pyrite Surface Condition

Figure 1 compares the changes in the zeta potential versus pH curve of pyrite (98.54%  $\text{FeS}_2$ ) measured in this study in ultra-pure deoxygenated water with the changes obtained in selected classical works that we briefly describe. The zeta potential versus pH curve of pyrite (95%  $\text{FeS}_2$ ) conditioned with argon measured by Fornasiero et al. [7] is the most negative of all the curves measured thus far according to our best knowledge. According to these authors, purging an aqueous solution with argon reduces the amount of dissolved oxygen to extremely low levels, which does not occur when purging with nitrogen, often used to limit oxidation. The surface of pyrite under an argon atmosphere has been suggested by Fornasiero and collaborators to be close to a virgin state. Little or no change in the zeta potential curve occurs at conditioning  $\text{pH} \geq 7$ , even if oxygen is present. Figure 1 also shows a zeta potential versus pH curve of pyrite (99.3%  $\text{FeS}_2$ ) obtained by López Valdivieso et al. [12] with the mineral conditioned open to the atmosphere. This curve replicated almost exactly the curve measured several years earlier by Fuerstenau et al. [28] who also conditioned the mineral and measured in atmospheric air. The curves by Fuerstenau et al. and López Valdivieso et al. show new additional isoelectric points, one at ca.  $\text{pH} 4.5$  and the other at ca.  $\text{pH} 6.4$ , which result from the oxidation of pyrite in this pH range. In the final stage of the oxidation of pyrite, there is agreement that the surface products generated correspond to ferric oxyhydroxides  $\text{Fe}(\text{O})\text{OH}$  of which goethite is one of the thermodynamically more stable forms and, thus, the surface of pyrite for  $\text{pH}$  between 4.5 and 6.4 is partially lined with ferric oxyhydroxide species. Simple iron hydroxides are intermediate oxidation products with a negative zeta potential over the entire pH range, Figure 1 shows, for example, the zeta potential changes versus pH curves for colloidal  $\text{Fe}(\text{OH})_2$  [29], which presents an isoelectric point at  $\text{pH} 6$  although the potential never becomes as positive as the curves of Fuerstenau et al. and López Valdivieso et al. The zeta potential of  $\text{Fe}(\text{OH})_3$  (not shown in Figure 1) also does not explain the positive zeta potential of oxidized pyrite because its value is always negative and very stable. However, the zeta potentials of colloidal precipitate of ferric oxyhydroxides [30] and of crystalline goethite [31] are positive and therefore can explain the positive zeta potential of oxidized pyrite; the zeta potential versus pH curves show an isoelectric point at  $\text{pH} 9.5$  and high positive values of zeta potential at  $\text{pH} \leq 9.5$ .

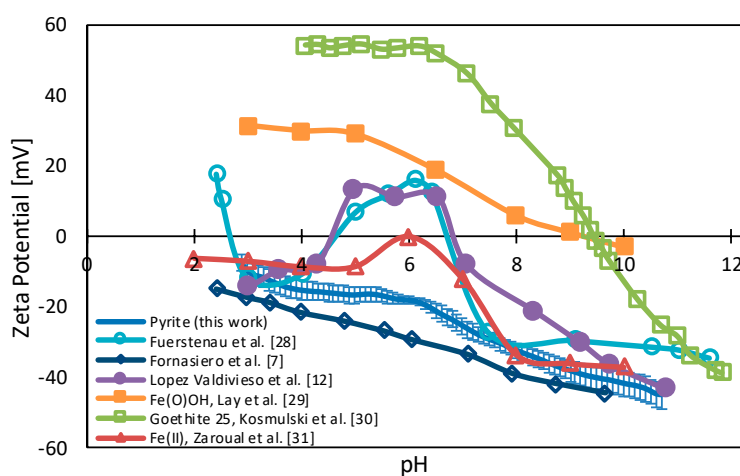


**Figure 1.** Zeta potential of pyrite as a function of pH, from different authors, under different oxidation degrees, and its comparison with different ferric species and states.

The presence of ferric oxyhydroxide species in isolated domains or patches on the otherwise virgin pyrite surfaces should be apparent when observing that its zeta potential versus pH curve is intermediate between the zeta potential curves of unoxidized pyrite and ferric oxyhydroxide species (see Figure 1), in the cases of Fuerstenau et al. [28] and López Valdivieso et al. [12]. In this work, a great effort was made so that the mineral had minimal exposure to air and that when it was unavoidable, it was for a minimal time. Our results in Figure 1 are interesting because they show that it was possible to limit the oxidation of the pyrite ore to a minimum at extreme values of pH. At intermediate pH, between 4 and 6, it is evident that the oxidation was somewhat higher, however the value of the zeta potential, in this case, remains high and negative, a clear indication that sites of unaltered pyrite control the zeta potential, a major difference with Fuerstenau et al. [28] and López Valdivieso et al. [12] in which cases the zeta potential was controlled by the oxidized sites.

### 3.2. Zeta Potentials and Adsorption Sequences

Figure 2 shows that ions of positive charge as those in the series  $\text{Cs}^+$ ,  $\text{K}^+$ ,  $\text{Na}^+$ , and  $\text{Li}^+$  act as counter ions on the negatively charged pyrite surface used here, adsorbing on the surface-dominating negative sites and, thus, decreasing the absolute value of the negative zeta potential. The figure also shows that the higher the cation concentration, the lower the absolute value of the zeta potential. Figure 3 shows that the magnitude of the negative zeta potential as a function of pH increases as the Hofmeister series [32], that is,  $\text{Cs}^+ > \text{K}^+ > \text{Na}^+ > \text{Li}^+$ . At first, it is perplexing that  $\text{Li}^+$ , with the highest charge density of all monovalent cations considered, is not the cation compressing the electrical double layer of pyrite most effectively; instead, we have  $\text{Cs}^+$  showing the highest effect.  $\text{Li}^+$ , the smallest ion in the series of monovalent cations located at one end of the Hofmeister series, renews the water molecules in its primary hydration shell relatively slower than the other cations of the monovalent series, which reduces its surface charge density and thus its screening power; the result is a low adsorption of  $\text{Li}^+$ , which occurs far from the surface. Results in Figures 2 and 3 can be explained by the “like absorbs like” concept borrowed from oxides [32,33]; that is, low isoelectric point surfaces preferentially adsorb poorly hydrated ions and high isoelectric point surfaces preferentially adsorb well-hydrated ions. Pyrite, aside from having a very low isoelectric point, is naturally hydrophobic with hydrophilic spots due to oxidation, and thus, hydration water is possible only in the spots and not in the rest of the surface. Thus, the thick hydration layer of  $\text{Li}^+$  “is not like” the hydration layer on the pyrite and, thus, Li ions remain relatively far from the pyrite surfaces. On the contrary,  $\text{Cs}^+$  ions, as pyrite, have very thin layers of hydration that are renewed very often, and thus adsorb closer to the mineral surface likely in bare state. Adsorption increases as the series  $\text{Cs}^+ > \text{K}^+ > \text{Na}^+ > \text{Li}^+$ . In the presence of monovalent alkali metal ions, the absolute value of the negative zeta potential of the pyrite follows the order  $\text{pyrite} > \text{Li}^+ > \text{Na}^+ > \text{K}^+ > \text{Cs}^+$ , which is even more pronounced as the ion concentration increases. The results with  $\text{LiCl}$  0.01 M (Figure 2) seem to defy the previous observation, especially at  $\text{pH} < 6$ , since the magnitude of the negative zeta potential of pyrite without electrolyte is clearly smaller than that of pyrite in aqueous solution of Li. A closer look at the results reveals that in the first case, there is an electrolyte present; this is Na from the pH regulator ( $\text{NaOH}$ ), which is better adsorbed than Li (from the  $\text{LiCl}$  0.01 M solution and the  $\text{LiOH}$  pH regulator). In this way, in the presence of salts, the scenario for the performance of a traditional collector as PAX radically changes. Despite all the efforts to avoid the oxidation of pyrite, working in atmospheres of permanently renewed nitrogen, Figure 2 shows that at pH 6 the generation of oxides in some small but sufficient extent is inevitable so that the pyrite adsorbs more cations and thereby reduces the absolute value of zeta potential more significantly.

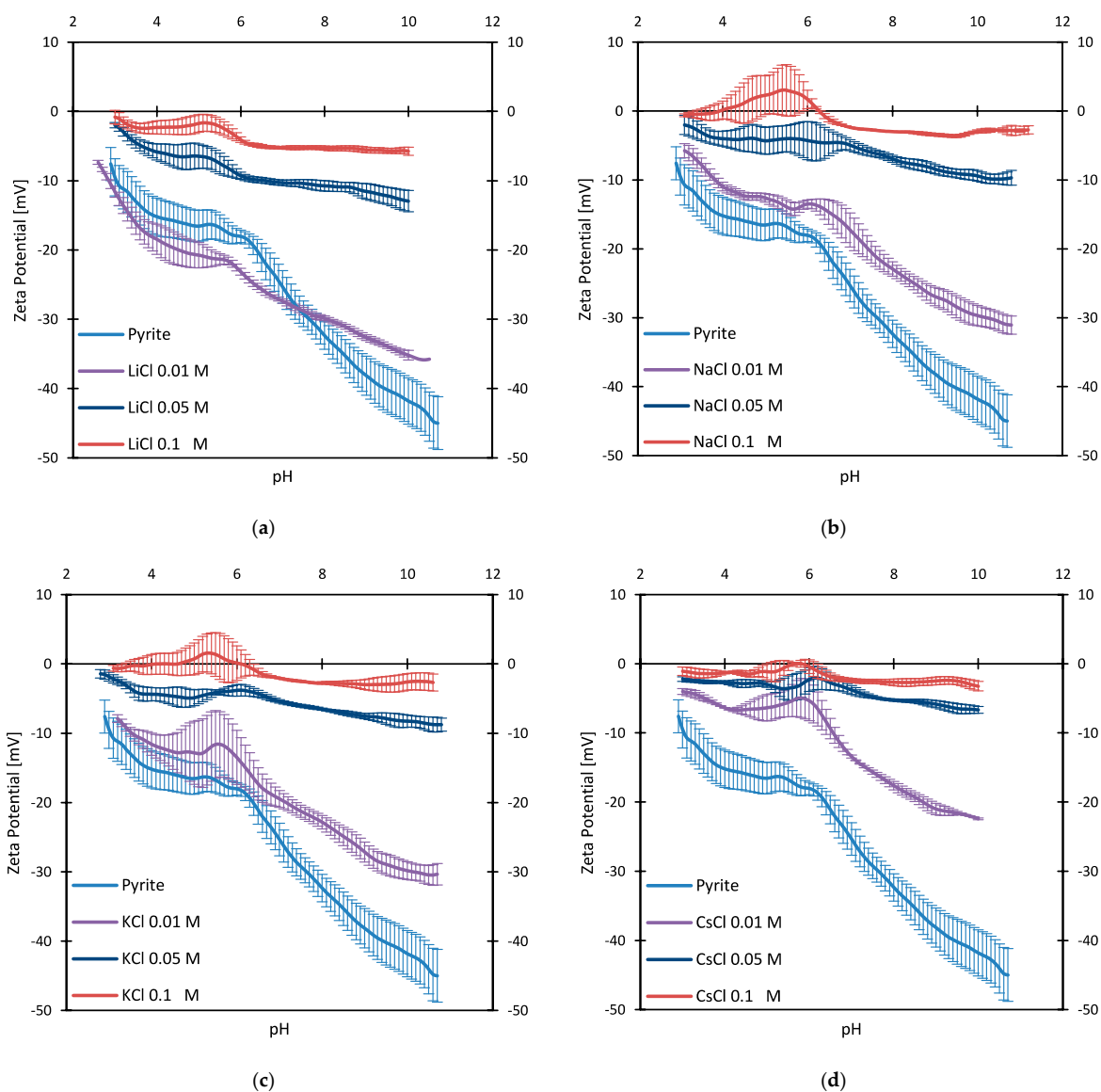


**Figure 2.** Zeta potential of pyrite as function of pH for different chloride salts of the monovalent alkaline metal series at increasing concentrations. (a) LiCl, (b) NaCl, (c) KCl, and (d) CsCl. Label Pyrite is omitted in curves for salts.

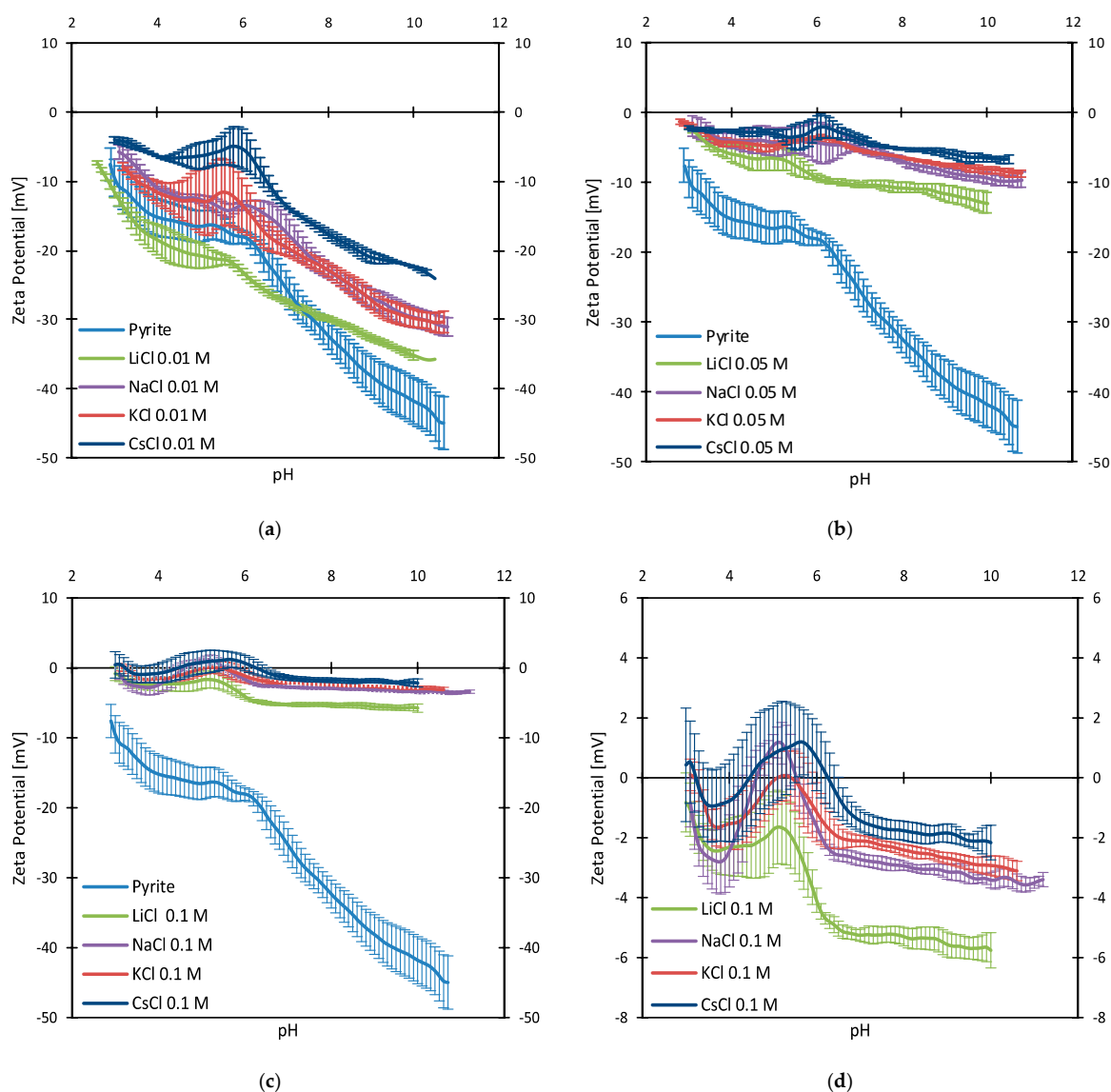
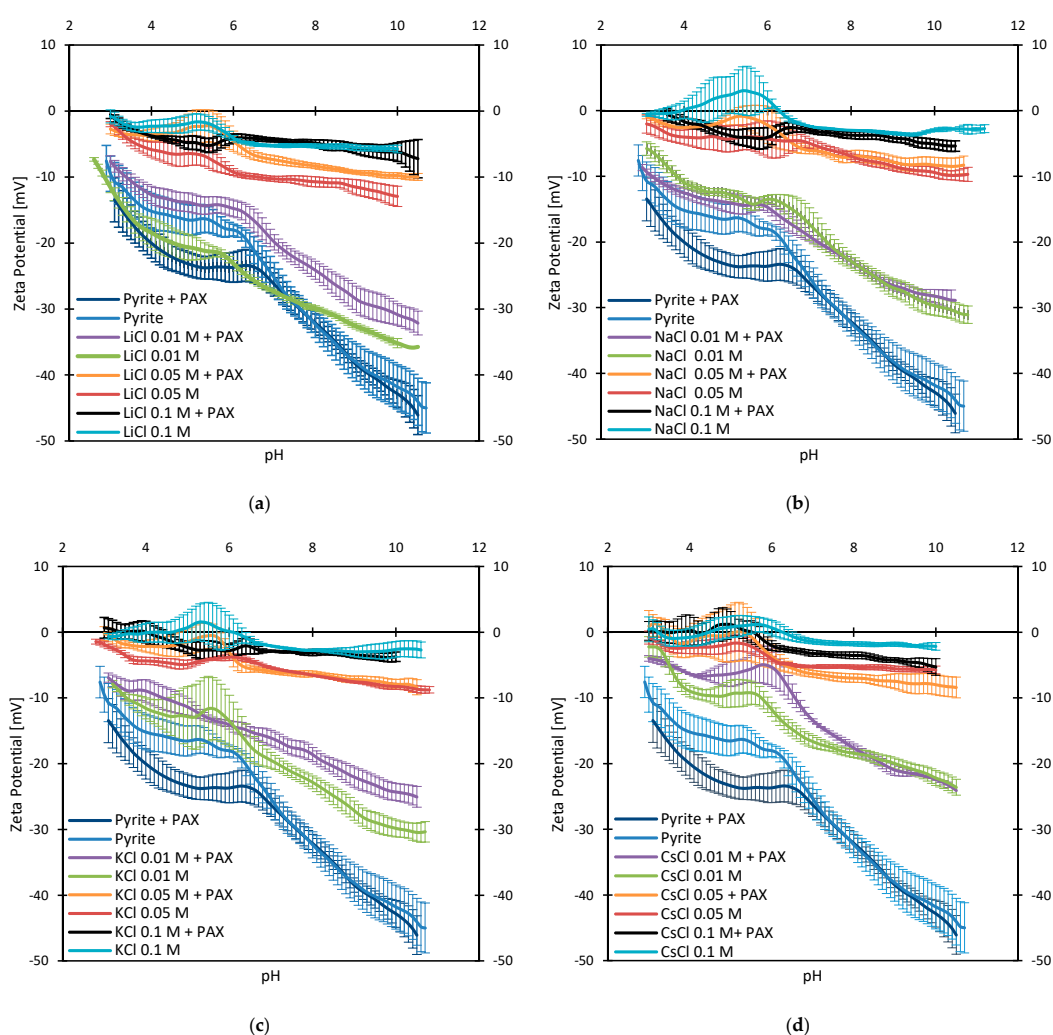


**Figure 3.** Zeta potential of pyrite as function of pH for different chloride salts of the monovalent alkaline metal series, comparison at concentrations (a) 0.01 M, (b) 0.05 M, (c) 0.1 M. Frame (d) is an enlarged view of Frame (c) to better distinguish the curves at the higher pH. Error bars are omitted for clarity but are available in Figure 1. Label Pyrite is omitted in curves for salts.

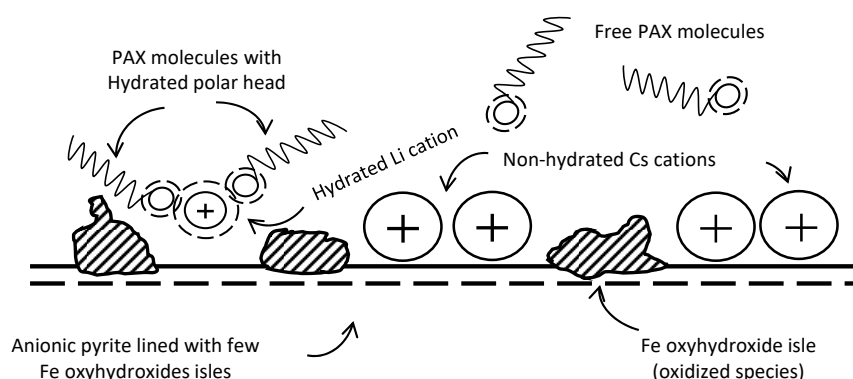
### 3.3. Zeta Potentials and the Effect of PAX

Figure 4 presents the change due to PAX in the zeta potential versus pH curve of pyrite previously equilibrated with monovalent metal cations in solution. Before entering the analysis of the interaction of PAX molecules and electrolytes at the pyrite surface, it is interesting to compare the zeta potential curve of pyrite with and without PAX in the absence of salts. In the low pH range,  $\text{pH} < 6$ , iron hydroxyl nuclei are born, which then grow on the surface of the pyrite either as continuous coating or discrete patches depending on in-situ conditions. Figure 4 shows that the addition of PAX leads to an increase in the magnitude of the negative zeta potential of the pyrite particles suggesting dissolution of the surface ferric hydroxides and recovery of bare pyrite, thus corroborating the theory of López Valdivieso et al. [12]. In the presence of salt, the pyrite surface exposed to the collector is constituted by a few oxidized sites, and many non-oxidized sites covered with monovalent cations by specific adsorption. Figure 4 shows that addition of the amyl xanthate collector at the concentration used and  $\text{pH} > 6$  (for which hydroxides interference is not expected) has little or no effect over the measured

zeta potential, except when Li is present. It seems that cations such as Na, K, and Cs under these conditions hampered adsorption of the collector, which would be detrimental for the floatation of pyrite. These results may be at the root of the poor pyrite recoveries we have obtained in flotation tests in the presence of monovalent cations (not reported here). Very different are the results with  $\text{Li}^+$  at every concentration ( $\leq 0.1$  M); when collector is added, the magnitude of the zeta potential decreases. The latter reminds us that strong water structure maker cations, which are used as pyrite activators, also decrease the magnitude of the zeta potential of pyrite in the order  $\text{Cu}^{2+} > \text{Fe}^{2+} \gg \text{Ca}^{2+} (>>> \text{Li}^+)$  [13,20,23]. The content of  $\text{Li}^+$  in seawater is very low, however it has been of great interest to include it in this study to identify, beyond doubt, the effect of the strongest monovalent cation on the zeta potential of pyrite exposed to collector, effects that could be more difficult to appreciate in the presence of cations that are less maker, such as  $\text{Na}^+$ . The decrease in magnitude of the zeta potential of pyrite in LiCl solution once PAX is added is explained as follows. On the one hand, Li ions promote structured water that has relatively higher viscosity than water in the presence of breaker cations [34,35]. Considering that  $\text{Li}^+$  is located (adsorbed) relatively farther from the surface of pyrite than the other cations from the series, and that it is less mobile due to the tight network of water that creates, it is ready for interaction with other molecules, PAX in particular. On the other hand, it is known that xanthate ligands participate in hydrogen bonding [36], which may even affect their chelating condition. Thus, the water network around the polar head of PAX molecules should be expected to be similar to that of hydrated  $\text{Li}^+$  cations facilitating the formation of a bond or linkage between them according to the concept of “like absorbs like” and, as a consequence, the formation of Li-mediated pyrite-PAX bridge. The stability of these bridges would be favored by the water network that hinders the movements of the  $\text{Li}^+$  cation and especially of the molecules of PAX. We speculate that these  $\text{Li}^+$ -mediated bridges lead to a xanthate shield around the anionic sites on the pyrite particles that decreases the magnitude of their zeta potential. This ability of  $\text{Li}^+$  is less pronounced in the other cations of the monovalent series. In Figure 4 it can be seen that  $\text{K}^+$  behaves like  $\text{Li}^+$  at least at a low concentration of K (0.01 M) and at  $\text{pH} > 6$ . However, this effect is due to the fact that the actual concentration of  $\text{K}^+$  is slightly higher due to the contribution of K from the collector. Figure 5 shows a schematic of the molecular configuration for each cation. The adsorption of xanthate anions directly onto the pyrite surface, as required for the mechanism proposed by López Valdivieso et al. [12], or onto oxidized spots on the pyrite surface, as invoked by Mermillod-Blondin et al. [11], are not shown in the schematic because, although present, they are not the controlling mechanism when the pyrite is carpeted with cations. Low concentration of cations ( $< 0.01$  M) favors formation of Li-mediated pyrite-PAX bridges. These bridges lead to xanthate shields around the anionic sites on the pyrite particles, thus increasing zeta potential. At higher concentrations, the surface is so lined with cations that PAX ceases to have a role on the surface of the pyrite and thus on the zeta potential. Likely, the same bridge mechanism is responsible for the decrease in magnitude of the negative zeta potential when metal ions such as  $\text{Cu}^{2+}$ ,  $\text{Fe}^{2+}$ , and  $\text{Ca}^{2+}$  are present, and most importantly, for the increase of pyrite floatability [20].



**Figure 4.** Zeta potential of pyrite as function of pH for different chloride salts of the monovalent alkaline metal series and concentrations with and without amyl xanthate (PAX). (a) LiCl, (b) NaCl, (c) KCl, and (d) CsCl. The concentration of PAX is always  $10^{-4}$  M. Label Pyrite is omitted in curves for salts.



**Figure 5.** Schematic of cation and PAX adsorption onto pyrite at the molecular level. Low concentration of cations ( $<0.01$  M) favors formation of Li-mediated pyrite–PAX bridges. At higher concentrations, the surface is so lined with cations that PAX ceases to have a role on the surface of the pyrite and, thus, on the zeta potential.

### 3.4. Zeta Potentials at Higher PAX Doses

An increased PAX dose amplifies the effect of  $\text{Li}^+$  as a pyrite activator but only at low salt concentrations. At high concentrations,  $>0.01$  M, PAX molecules do not find room to percolate to the surface of the pyrite. At low salt concentrations,  $<0.01$  M, Figure 6 shows that the activating effect of Li is apparent, and that a slight activating effect of  $\text{Na} > \text{K} > \text{Cs}$  appears. Clearly, the interaction of pyrite with PAX in the presence of salts obeys rules different than those anticipated by Lopez Valdivieso et al. [12] and Mermillod-Blondin et al. [11]. Figure 7 compares the changes in the zeta potential versus pH curve of pyrite for different chloride salts at 0.01 M and PAX at  $10^{-4}$  and  $10^{-3}$  M. It is interesting to add to the comparison the changes in the zeta potential versus pH curve at the same salt concentration but in the absence of PAX (Figure 3a). We see that the zeta potential in the presence of  $\text{Li}^+$  shows the major changes, decreasing in magnitude from the curve with no PAX to the curve with the highest dose of PAX. The zeta potential in the presence of the other cations also decreases, but not in the magnitude measured in the presence of  $\text{Li}^+$ . Finally, at low salt concentrations and at the highest dose of PAX tested here, zeta potential versus pH curves for all cations tend to collapse into a single curve. At salt concentrations higher than 0.01 M, PAX at any dose is unable to reach the surface of the pyrite and therefore the zeta potential versus pH curve is determined by the cations and not by PAX. Increasing PAX over  $10^{-3}$  M at low salt concentrations may decrease the magnitude of the zeta potential, albeit marginally.

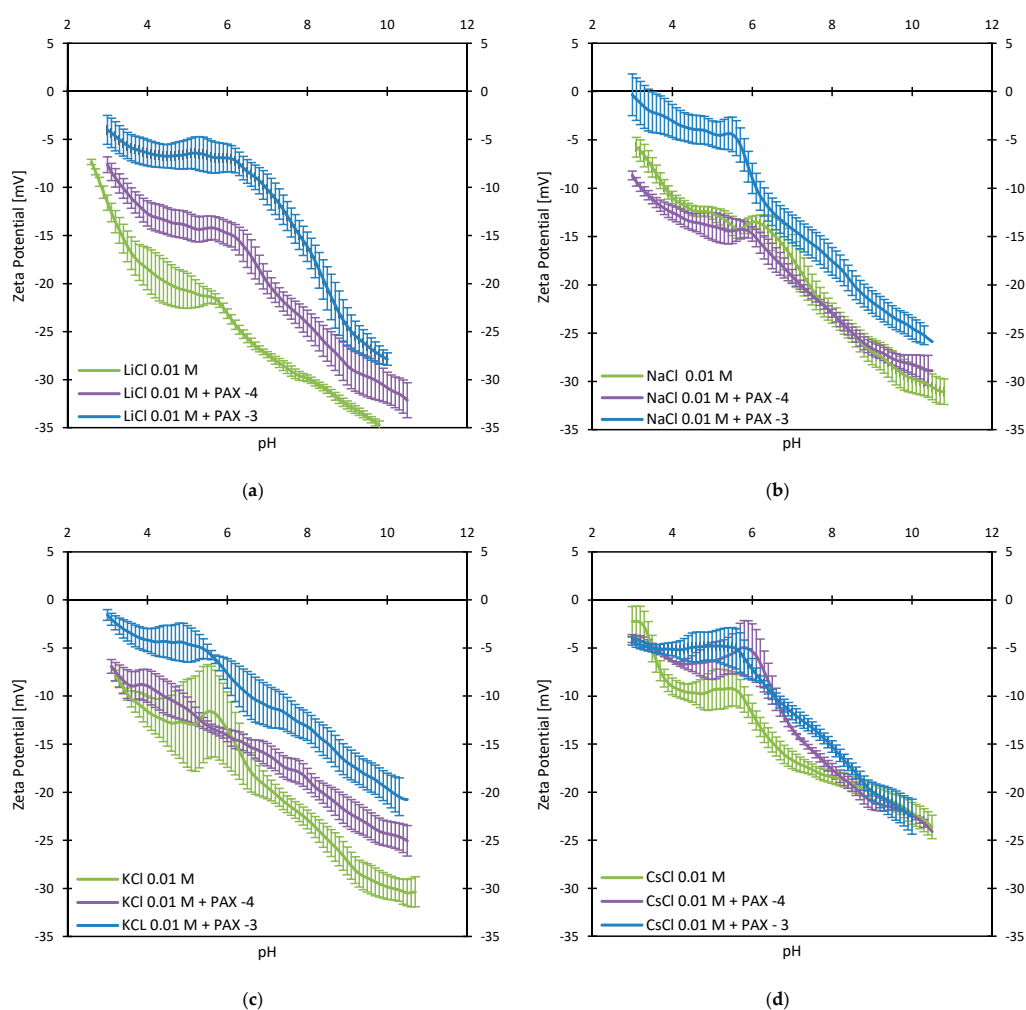


**Figure 6.** Zeta potential of pyrite as function of pH for different chloride salts and different concentrations of amyl xanthate (PAX). (a) LiCl, (b) NaCl, (c) KCl, and (d) CsCl. Concentrations of PAX are 0 M,  $10^{-4}$  M (−4), and  $10^{-3}$  M (−3).

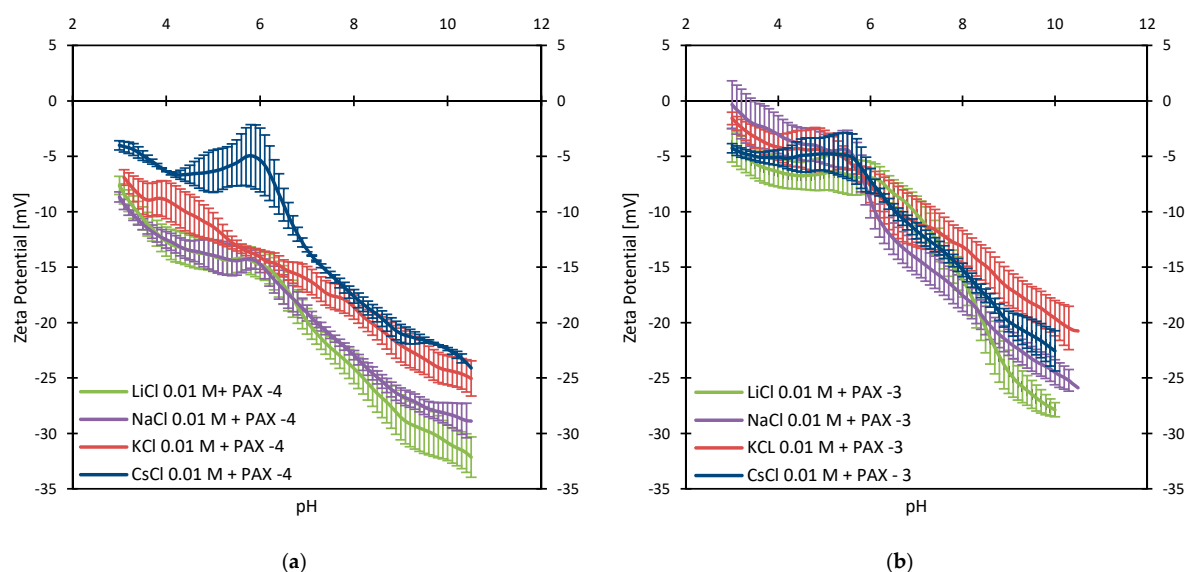


**Figure 7.** Zeta potential of pyrite as function of pH for different chloride salts at two concentrations of amyl xanthate (PAX) (a)  $10^{-4}$  M (-4) and (b)  $10^{-3}$  M (-3).

#### 4. Conclusions

The presence of monovalent alkali metal chloride salts offers such a new scenario for the interaction of pyrite and collector in aqueous media that existing theories about mechanisms of pyrite oxidation, collector adsorption, and reaction mechanisms may need to be revisited. The magnitude of the negative zeta potential as a function of pH follows the inverse Hofmeister series, that is,  $\text{Cs}^+ < \text{K}^+ < \text{Na}^+ < \text{Li}^+$ . Addition of PAX in the absence of salts leads to an increase in magnitude of the zeta potential of the pyrite particles, suggesting the dissolution of the surface ferric hydroxides and recovery of bare pyrite, thus corroborating existing theories. In the presence of salt, the addition of PAX at  $\text{pH} > 6$  has little or no effect over the measured zeta potential, except when  $\text{Li}^+$  is present. We speculate that these Li-mediated bridges lead to a xanthate shield around the anionic sites on the pyrite particles that decreases the magnitude of their zeta potential. An increased PAX dose amplifies the effect of Li as a pyrite activator, but only at low salt concentrations. At high concentrations,  $>0.01$  M, the PAX molecules do not find room to percolate to the surface of the pyrite. This new knowledge coupled should help to improve the current understanding of the flotation processes of copper ore in the presence of pyrite in saline water.

**Author Contributions:** A.P. and P.G.T. conceived and designed the experiments; A.P. and S.M.A. performed the experiments; A.P., S.M.A., and P.G.T. analyzed the data; L.G. and P.G.T. contributed reagents/materials/analysis tools; A.P., S.M.A., and P.G.T. wrote the paper.

**Funding:** This research was funded by Centro CRHIAM Project Conicyt/Fondap/15130015.

**Acknowledgments:** We gratefully acknowledge the financial support of Centro CRHIAM Project Conicyt/Fondap/15130015.

**Conflicts of Interest:** The authors declare no conflict of interest.

#### References

1. Castro, S.; Laskowski, J.S. Froth flotation in saline water. *KONA Powder Part. J.* **2011**, *29*, 4–15. [[CrossRef](#)]
2. Fuerstenau, M.C.; Kuhn, M.C.; Elgillani, D.A. The role of dixanthogen in xanthate flotation of pyrite. *Trans. Soc. Min. Eng. AIME* **1968**, *241*, 148–156.
3. Healy, T.W.; Moignard, M.S. A review of electrokinetic studies of metal sulphides. In *Flotation-A.M. Gaudin Memorial Volume*; Fuerstenau, M.C., Ed.; American Institute of Mining, Metallurgical, and Petroleum Engineers: New York, NY, USA, 1976.

4. Leppinen, J.O. FTIR and flotation investigation of the adsorption of ethyl xanthate on activated and non-activated sulfide minerals. *Int. J. Miner. Process.* **1990**, *30*, 245–263. [[CrossRef](#)]
5. Montalti, M.; Fornasiero, D.; Ralston, J. Ultraviolet-visible spectroscopic study of the kinetics of adsorption of ethyl xanthate on pyrite. *J. Colloid Interf. Sci.* **1991**, *143*, 440–450. [[CrossRef](#)]
6. Smart, R.S.C. Surface layers in base metal sulphide flotation. *Miner. Eng.* **1991**, *4*, 891–909. [[CrossRef](#)]
7. Fornasiero, D.; Eijt, V.; Ralston, J. An electrokinetic study of pyrite oxidation. *Colloid Surface* **1992**, *62*, 63–73. [[CrossRef](#)]
8. Richardson, P.E. Surface chemistry of sulphide flotation. In *Mineral Surfaces, The Mineral Society Series No. 5*; Vaughan, D.J., Pattick, R.A.D., Eds.; Chapman and Hall: London, UK, 1995; pp. 261–302.
9. Shannon, L.K.; Trahar, W.J. The role of collector in sulfide ore flotation. In *Advances in Mineral Processing*; Somasundaran, P., Ed.; Soc. Mining Engineers of AIME, Inc.: Littleton, CO, USA, 1986; pp. 408–425.
10. Smart, R.S.C.; Amarantidis, J.; Skinner, W.; Prestidge, C.A.; La Vanier, L.; Grano, S. Surface analytical studies of oxidation and collector adsorption in sulphide mineral flotation. *Scanning Microscopy* **1998**, *12*, 553–583.
11. Mermillod-Blondin, R.; Kongolo, M.; de Donato, P.; Benzaazoua, M.; Barrès, O.; Bussière, B.; Aubertin, M. Pyrite flotation with xanthate under alkaline conditions-application to environmental desulfurization. In *Centenary of Flotation Symposium Brisbane, Queensland*; Johnson, G.J., Ed.; Australasian Institute of Mining and Metallurgy: Brisbane, Australia, 2005; pp. 683–692.
12. Lopez-Valdivieso, A.; Sánchez Lopez, A.A.; Song, S. On the cathodic reaction coupled with the oxidation of xanthates at the pyrite/aqueous solution interface. *Int. J. Miner. Process.* **2005**, *77*, 154–164. [[CrossRef](#)]
13. He, S.; Fornasiero, D.; Skinner, W. Correlation between copper-activated pyrite flotation and surface species: Effect of pulp oxidation potential. *Miner. Eng.* **2005**, *18*, 1208–1213. [[CrossRef](#)]
14. He, S. Depression of Pyrite in Flotation of Copper Ores. Ph.D. Thesis, University of South Australia, Adelaide, SA, Australia, 2006.
15. Chandra, A.P.; Gerson, A.R. The mechanisms of pyrite oxidation and leaching: A fundamental perspective. *Surf. Sci. Rep.* **2010**, *65*, 293–315. [[CrossRef](#)]
16. Buckley, A.N.; Woods, R. The surface oxidation of pyrite. *Appl. Surf. Sci.* **1987**, *27*, 437–452. [[CrossRef](#)]
17. Buckley, A.N.; Hamilton, I.C.; Woods, R. Investigation of the surface oxidation of sulfide minerals by linear potential sweep voltammetry and X-ray photoelectron spectroscopy. In *Flotation of Sulfide Minerals*; Forssberg, K.S.E., Ed.; Elsevier: Amsterdam, The Netherlands, 1985; pp. 41–60.
18. Knipe, S.W.; Mycroft, J.R.; Pratt, A.R.; Nesbitt, H.W.; Bancroft, G.M. X-ray photoelectron spectroscopic study of water adsorption on iron sulphide minerals. *Geochim. Cosmochim. Ac.* **1995**, *59*, 1079–1090. [[CrossRef](#)]
19. Smart, R.S.C.; Amarantidis, J.; Skinner, W.M.; Prestidge, C.A.; La Vanier, L.; Grano, S.R. Surface analytical studies of oxidation and collector adsorption in sulfide mineral flotation. In *Solid-Liquid Interfaces; Topics in Applied Physics*; Wandelt, K., Thurgate, S., Eds.; Springer-Verlag: Berlin/Heidelberg, Germany, 2003; Volume 85, pp. 3–62.
20. Zhang, Q.; Xu, Z.; Bozkurt, V.; Finch, J.A. Pyrite flotation in the presence of metal ions and sphalerite. *Int. J. Miner. Process.* **1997**, *52*, 187–201. [[CrossRef](#)]
21. Miller, J.D.; Kappes, R.; Simmons, G.L.; LeVier, K.M. Pyrite activation in amyl xanthate flotation with nitrogen. *Miner. Eng.* **2006**, *19*, 659–665. [[CrossRef](#)]
22. Pecina, E.T.; Uribe, A.; Nava, F.; Finch, J.A. The role of copper and lead in the activation of pyrite in xanthate and non-xanthate systems. *Miner. Eng.* **2006**, *19*, 172–179. [[CrossRef](#)]
23. Chandra, A.P.; Gerson, A.R. A review of the fundamental studies of the copper activation mechanisms for selective flotation of the sulfide minerals, sphalerite and pyrite. *Adv. Colloid Interface* **2009**, *145*, 97–110. [[CrossRef](#)] [[PubMed](#)]
24. Anderson, C.D. Fundamentals of rare earth flotation surface chemistry: Elektrokinetic phenomena. *Min. Metall. Explor.* **2014**, *31*, 176. [[CrossRef](#)]
25. Ruiz-Agudo, E.; Burgos-Cara, A.; Ruiz-Agudo, C.; Ibañez-Velasco, A.; Cölfen, H.; Rodríguez-Navarro, C. A non-classical view on calcium oxalate precipitation and the role of citrate. *Nat. Commun.* **2017**, *8*, 1–10. [[CrossRef](#)]
26. Nduwa-Mushidi, J.; Anderson, C.G. Surface Chemistry and Flotation Behaviors of Monazite-Apatite-Ilmenite-Quartz-Rutile-Zircon with Octanohydroxamic Acid. *J. Sustain. Metall.* **2017**, *3*, 62–72. [[CrossRef](#)]

27. Zolezzi, C.; Ihle, C.F.; Angulo, C.; Palma, P.; Palza, H. Effect of the oxidation degree of graphene oxides on their adsorption, flocculation, and antibacterial behavior. *Ind. Eng. Chem. Res.* **2018**, *57*, 15722–15730. [[CrossRef](#)]
28. Fuerstenau, M.C.; Natalie, C.A.; Rowe, R.M. Xanthate adsorption on selected sulfides in the virtual absence and presence of oxygen: Part II. *Int. J. Miner. Process.* **1990**, *29*, 111–119. [[CrossRef](#)]
29. Lay, M.L.; Wu, H.M.; Huang, C.H. Study of the zeta potential of Fe(O)OH colloids. *J. Mater. Sci.* **1995**, *30*, 5473–5478. [[CrossRef](#)]
30. Kosmulski, M.; Maczka, E.; Jartych, E.; Rosenholm, J.B. Synthesis and characterization of goethite and goethite-hematite composite: Experimental study and literature survey. *Adv. Colloid Interf.* **2003**, *103*, 57–76. [[CrossRef](#)]
31. Zaroual, Z.; Azzi, M.; Saib, N.; Chainet, E. Contribution to the study of electrocoagulation mechanism in basic textile effluent. *J. Hazard. Mat.* **2006**, *131*, 73–78. [[CrossRef](#)] [[PubMed](#)]
32. Franks, G.V. Zeta potentials and yield stresses of silica suspensions in concentrated monovalent electrolytes: Isoelectric point shift and additional attraction. *J. Colloid Interf. Sci.* **2002**, *249*, 44–51. [[CrossRef](#)] [[PubMed](#)]
33. Jeldres, R.I.; Toledo, P.G.; Concha, F.; Stickland, A.D.; Usher, S.P.; Scales, P.J. Impact of seawater salts on the viscoelastic behavior of flocculated mineral suspensions. *Colloid Surface A* **2014**, *461*, 295–302. [[CrossRef](#)]
34. Hancer, M.; Celik, M.S.; Miller, J.D. The significance of interfacial water structure in soluble salt flotation systems. *J. Colloid Interf. Sci.* **2001**, *235*, 150–161. [[CrossRef](#)] [[PubMed](#)]
35. Marcus, Y. Effect of ions on the structure of water. *Pure Appl. Chem.* **2010**, *82*, 1889–1899. [[CrossRef](#)]
36. Walters, M.C.; Barad, J.; Sireci, A.; Golen, J.A.; Rheingold, A.L. Xanthate sulfur as a hydrogen bond acceptor: The free xanthate anion and ligand sulfur in nickel tris ethylxanthate. *Inorg. Chim. Acta* **2005**, *358*, 633–640. [[CrossRef](#)]



© 2019 by the authors. Licensee MDPI, Basel, Switzerland. This article is an open access article distributed under the terms and conditions of the Creative Commons Attribution (CC BY) license (<http://creativecommons.org/licenses/by/4.0/>).